PENNSTATE

FUNDAMENTAL PHENOMENA ON FUEL DECOMPOSITION AND BOUNDARY LAYER COMBUSTION PROCESSES WITH APPLICATIONS TO HYBRID ROCKET MOTORS

Semiannual Progress Report

Part 1

Kenneth K. Kuo, Y. C. Lu, Martin J. Chiaverini, George C. Harting
The Propulsion Engineering Research Center
The Pennsylvania State University
University Park, PA 16802

Summary:

An experimental study on the fundamental processes involved in fuel decomposition and boundary layer combustion in hybrid rocket motors is being conducted at the High Pressure Combustion Laboratory of the Pennsylvania State University. This research should provide a useful engineering technology base in the development of hybrid rocket motors as well as a fundamental understanding of the complex processes involved in hybrid propulsion. A high pressure slab motor has been designed and manufactured for conducting experimental investigations. Oxidizer (LOX or GOX) supply and control systems have been designed and partly constructed for the head–end injection into the test chamber. Experiments using HTPB fuel as well as fuels supplied by NASA designated industrial companies will be conducted. Design and construction of fuel casting molds and sample holders have been completed. The portion of these items for industrial company fuel casting will be sent to the McDonnell Douglas Aerospace Corporation in the near future. The study focuses on the following areas: observation of solid fuel burning processes with LOX or GOX, measurement and correlation of solid fuel regression rate with operating conditions, measurement of flame temperature and radical species concentrations, determination of the solid fuel subsurface temperature profile, and utilization of experimental data for validation of a companion theoretical study (Part 2) also being conducted at PSU.

Hybrid Motor Analog:

Hybrid rocket systems offer several advantages over their liquid and solid rocket counterparts. First, hybrid rockets require only half as much feed system hardware as liquid propellant rockets, and therefore display improved reliability. Second, since they are much less sensitive to cracks and imperfections in the solid fuel grain, hybrids have safety advantages over solid propellant rockets. Third, hybrid rockets can be throttled for thrust control and maneuvering. In addition, solid fuels are safer for manufacture, transportation, and storage. From a performance standpoint, hybrid rockets have specific impulse similar to those of liquid and solid rocket motors.

The experimental hybrid rocket program at PSU has been established to study the fundamental fuel decomposition and reacting boundary–layer processes (see Fig. 1) which occur in actual hybrid rocket motors or motor analogs. Figure 2 shows a schematic diagram of the overall hybrid test rig, including motor analog, gas supply system, and ignition system. A design–analysis computer code was developed to assist the design of the test motor. The code used a time–dependent continuity equation coupled with a chemical equilibrium transport code (CET–86) to determine fuel regression rate, oxidizer–to–fuel mass ratio, chamber pressure, and gas temperature. Prior to the final selection of test motor dimensions, parametric studies were conducted to determine the effect of oxidizer flow rate, nozzle diameter, test time, and fuel composition on motor operating characteristics in order to meet the proper range of test conditions. Based upon the results of parametric studies and experience from previous experiments at Penn State, a windowed, 2–D hybrid motor was designed. Figure 3 shows four views of the hybrid motor analog in two different configurations. The top drawings in Figure 3 show the main chamber section in the absence of the window assemblies, while the lower drawings illustrate the fully assembled motor with windows, window holders, and window retainers in place. Figure 4 shows a photograph of the main chamber section. The motor is constructed of stainless steel and weighs approximately 700 lbs. It has an overall length of 42 in, width of 7 in, and height of 10 in. The motor utilizes either two opposing fuel slabs or one fuel slab with an opposing inert slab and may operate with either gaseous or liquid oxygen as the oxidizer source. Interchangeable exit nozzles provide partial control of chamber pressure. The two sets of opposing windows can accommodate a variety of instrumentation and diagnostics for measuring fuel regression rate, gas velocity, flame temperature, and species concentrations. The motor has been constructed, delivered to the High Pressure Combustion Laboratory, and installed on a test stand. The test stand consists mainly of a steel plate bolted to three wide–flanged steel I beams, which are connected to an existing steel frame. The windowed hybrid motor is mounted rigidly to the test stand, with its thrust transmitted to several components of the stand, during operation.

Figures 5 through 11 show various components of the motor. The window holders fit into the cavities on either side of the main chamber section such that their outer surfaces are flush with the sides of the main chamber, and secure the windows during testing. The window retainers are bolted to the sides of the main chamber section during testing and serve to hold the windows and window holders in place. In addition to the quartz window shown in Fig. 7, Lexan, gaphite, and steel windows will also be utilized during various tests. For visualization studies, an inner quartz window will be used with an outer Lexan window which provides mechanical strength. During X–ray, or other non–visualization tests, an inner graphite window and outer steel window will be used.

The gaseous oxygen injector shown in Fig. 8 fits through a threaded hole in the head end

of the motor, and is held in place with a compression fitting. The graphite pre–nozzle mixing chamber shown in Fig. 9 fits into the aft–end of the motor and protects the interior metal surfaces when the hot combustion gases flow through the chamber and the nozzle. The graphite nozzle shown in Fig. 10 is held in place by an exterior retaining ring. Figure 11 shows an inert graphite sample which replaces one of the fuel slabs during the single fuel slab tests of fast–burning, industrial fuels.

Figure 12 provides an exploded view of a large portion of the motor analog, including windows, window holders, window retainers, GOX injector, and exit nozzle. The steel, graphite, and Lexan windows mentioned above are also shown, as is the exit nozzle retaining ring at the aft end of the chamber.

Gaseous Oxygen Supply System:

The gaseous oxygen supply system shown in Fig. 2 consists of a main feed line and a nitrogen purge. Remotely operated ball valves initiate and terminate the flow of oxygen, while a critical flow venturi maintains a steady mass flux through the main line. An upstream thermocouple and pressure transducers located on either side of the venturi give a measure of the oxygen flow rate. The flow rate will be preset for each test. Filters in the GOX and GN_2 supply lines prevent contamination of the system. Construction of the GOX supply system is nearing completion.

Ignition System:

Based upon a literature search and comparative study of various ignition systems, an igniter was designed as shown in Fig. 2. The ignition system consists of a pair of high–pressure gaseous oxygen/methane pre–mixed torches and a pair of solid–propellant pilot flames. For clarity, only one torch and pilot flame are shown in Fig. 2. The other pair branch off from the main lines and enter the chamber from above. Flashback arresters prevent flashback from occuring in the pre–mixed sections of the igniter lines. The solid propellant strands are ignited electrically using nichrome wires connected to an AC transformer. Remotely operated solenoid valves control the flow of oxygen and methane. Check valves and vents prevent the contamination of the gas bottles and over pressurization of the system. Gaseous nitrogen is used to purge the ignition system after each test. The ignition system has been constructed and tested successfully with feed pressures up to 550 psig.

Liquid Oxygen Injector:

After a thorough literature search on spray injectors, a showerhead design was considered for the LOX injector. This design employs multiple rows of pressure atomized jets aligned parallel

to the fuel slab(s). This type of design has been well studied, and such an injector is relatively easy to manufacture. A prototype single–row injector was constructed and tested in an existing pressure chamber. Flow visualization studies using a video camera and a strobe light have been conducted to observe the break–up characteristics and degree of atomization of a water jet through the injector. This study is helpful in selecting the appropriate hole size and injector spacing for the pre–specified range of feed pressures.

Control and Diagnostic Systems:

A control panel for operating the hybrid motor, GOX supply line, and ignition system has been designed and assembled. The control panel will display a mimic diagram of the entire hybrid motor analog system, as well as switches to arm the GOX supply and ignition system, and to control the various remote valves and the solid propellant pilot flames. The tests will be automated using an IBM PC/AT computer and data acquisition and control board. The control program is currently being written and tested.

Several diagnostic techniques will be used to measure the properties of interest. The fuel regression rate will be deduced from images obtained by a high speed camera coupled with a real–time X–ray radiography system (see Fig. 13). Radical species (such as OH) concentration and flame temperature will be measured as a function of longitudinal location using UV/visible absorption spectroscopy. Both static and dynamic pressures in the motor will be measured using pressure transducers.

The subsurface temperature of the solid fuel will be measured by an array of R–type fine–wire thermocouples which are embedded at pre–determined depths along the solid fuel slabs prior to testing (see Fig. 14). Since the micro–thermocouples are easily damaged, it is expected that casting them inside small fuel plugs, then casting the plugs inside the fuel slab, will produce better results than simply inserting the thermocouples into the fuel while it is curing. Therefore, 25μm micro–thermocouples will be made, soldered to extension wires, and cast inside 0.25 inch diameter fuel plugs. Seven thermocouple–containing fuel plugs will be cast into each HTPB fuel slab.

Solid Fuels and Fuel Molds:

In order to fabricate solid fuels with high quality and to achieve short curing time, several fuel curing tests were conducted in a small, practice mold using R–45M homopolymer from Elf Atochem and a curing agent of Isonate 143L (MDI) from Dow Chemical Co. Since R–45M has a hydroxyl value of about 0.73 meq/g and Isonate 143L has an amine equivalence of 144.3 g/eq, the weight of Isonate 143L used was approximately equal to 11% of the weight of R–45M (assuming an NCO/OH ratio of 1.05). The fuel curing time was about 8 hours, nearly an order of magnitude shorter compared to the combination of R–45M, IPDI curing agent, and dibutyltin dilaurate

catalyst. Approximately 35 gallons of R–45M have been received from Elf Atochem to cast the fuel slabs for motor tests using HTPB fuel processed at the Penn State University.

Dr. David Dean from the McDonnell Douglas Aerospace Corporation arrived on Sept. 15 for a discussion of fuel casting techniques. After examining the fuel molds and sample holders that will be used to cast the fuel slabs for the hybrid tests, Dr. Dean suggested some slight modifications to the molds. The modifications included plugging a pair of holes in the base of the molds which were designed to inject the fuel in its liquid state. Dr. Dean felt that this procedure would be very difficult because of the high viscosity of some solid fuels. Instead, he suggested that the fuel be poured into the mold from one end wall of the mold. After all the bubbles had escaped, this end wall will be mounted and the fuel allowed to cure. He also discussed aspects of his own solid fuel experiments.

The fuel molds were modified based on Dr. Dean's suggestions, then shipped, along with the sample holders, to Hitemco Southwest for Teflon coating. The treated molds and sample holders recently arrived back at the High Pressure Combustion Lab. Several fuel slabs have been successfully cured in the molds, demonstrating that the Teflon coating works quite well as a release agent. The fuel molds and sample holders required by industrial companies will soon be shipped to McDonnell Douglas Aerospace Corp.

Future Work:

Testing of the hybrid motor analog will commence after the control system has been completed and diagnostic equipment, such as pressure transducers and thermocouples, installed. Table 1 shows the range of proposed test parameters. The first series of tests will utilize solid HTPB fuel and GOX. Later tests will use fuels supplied by industry. After all tests with GOX have been completed, the chamber will be moved into the Cryogenic Laboratory at the High Pressure Combustion Lab in order to use the existing LOX supply and control system for LOX/solid fuel tests. The possibility of using a recently received hybrid test rig from Mr. Leon Strand of JPL for LOX/solid fuel tests is being considered.

Table 1. Range of Test Parameters

Solid Fuel Composition:	Baseline HTPB and NASA Fuels
Chamber Pressure:	300–900 psi
Oxidizer Flow Rate:	up to 1.5 lb/s
Initial Temperature:	70° F nominal
	35° F low
	90° F high

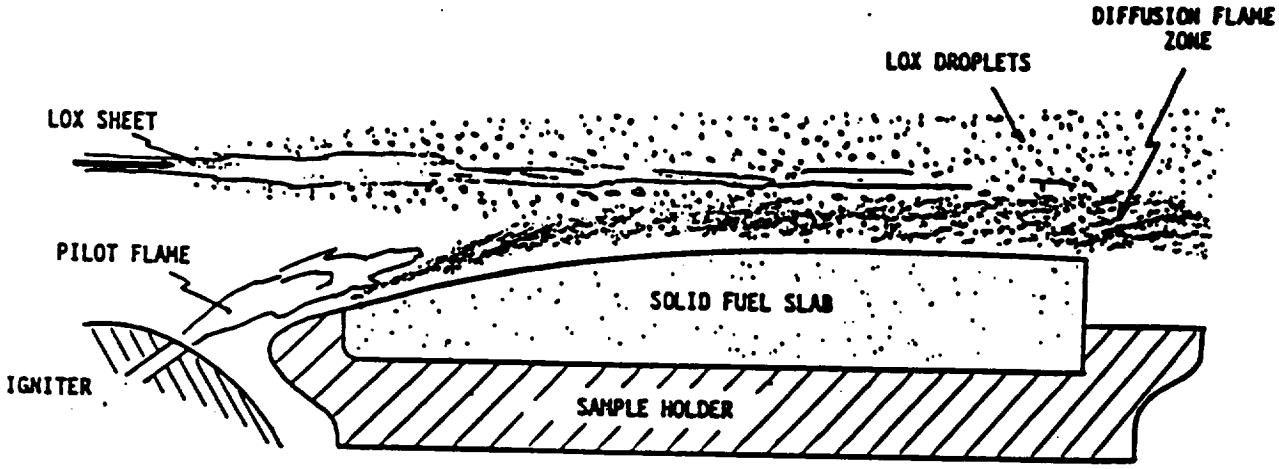

Fig. 1 Schematic Diagram of the Diffusion Flame Zone Adjacent to the Solid Fuel Slab

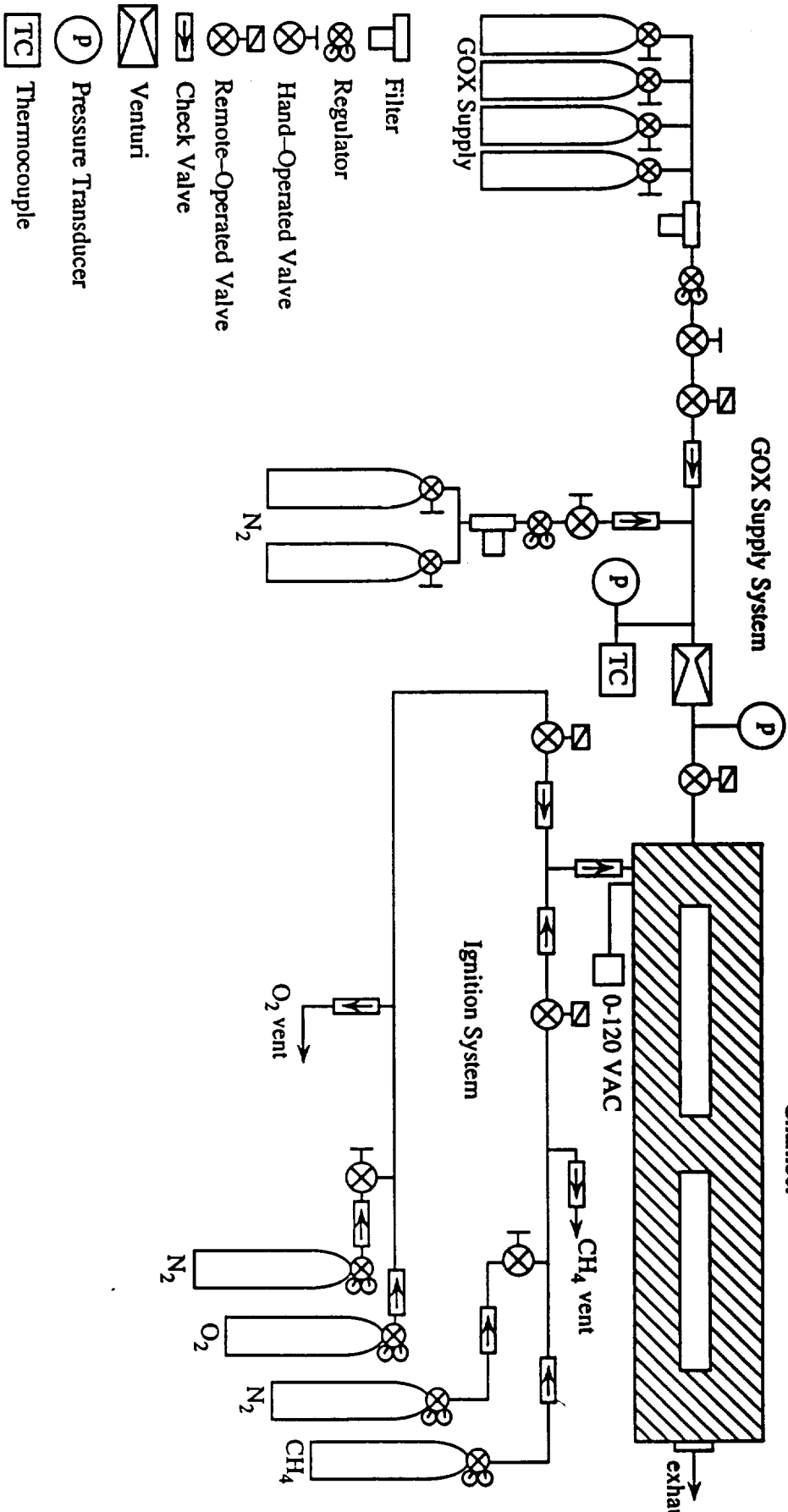

Figure 2. Penn State Hybrid Test Rig

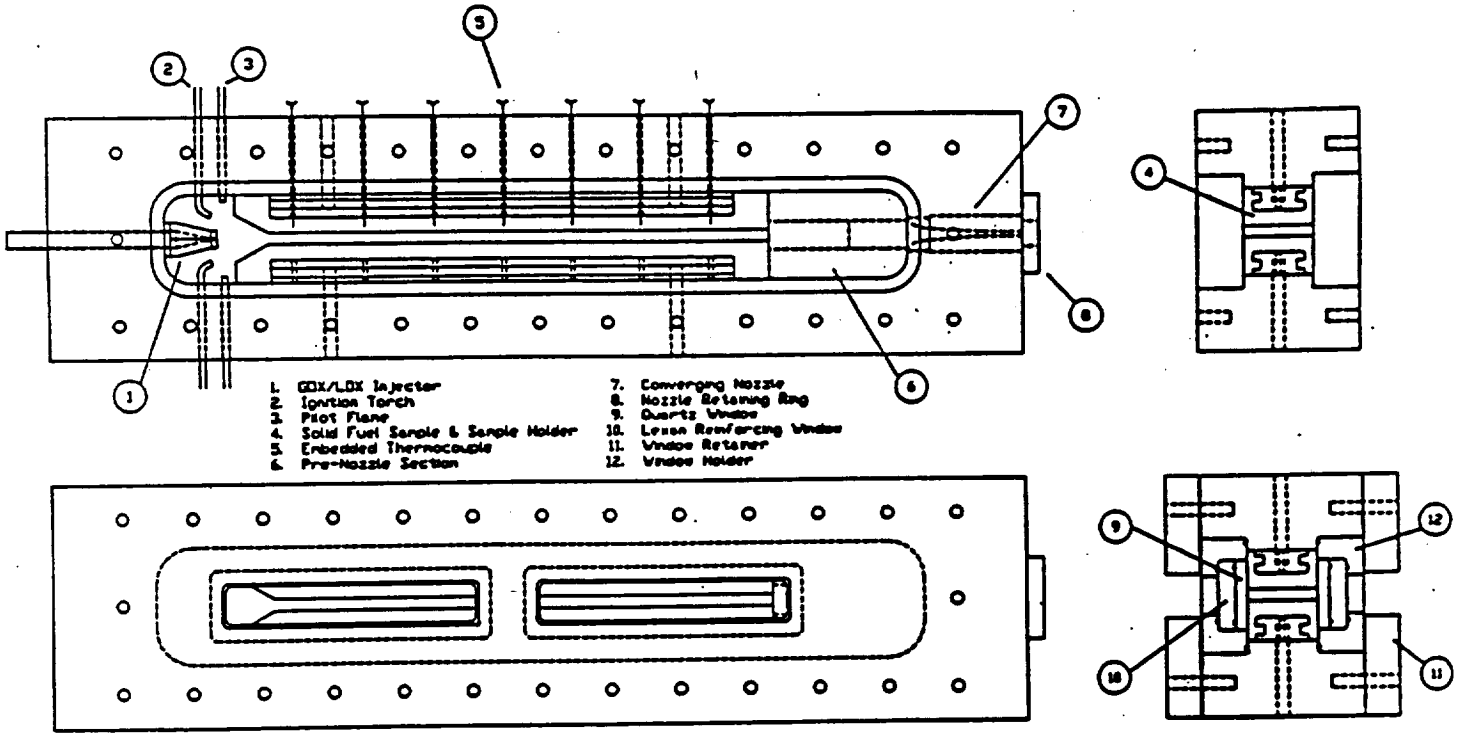

Fig. 3 - Partial Assembly Drawing of Hybrid Test Chamber

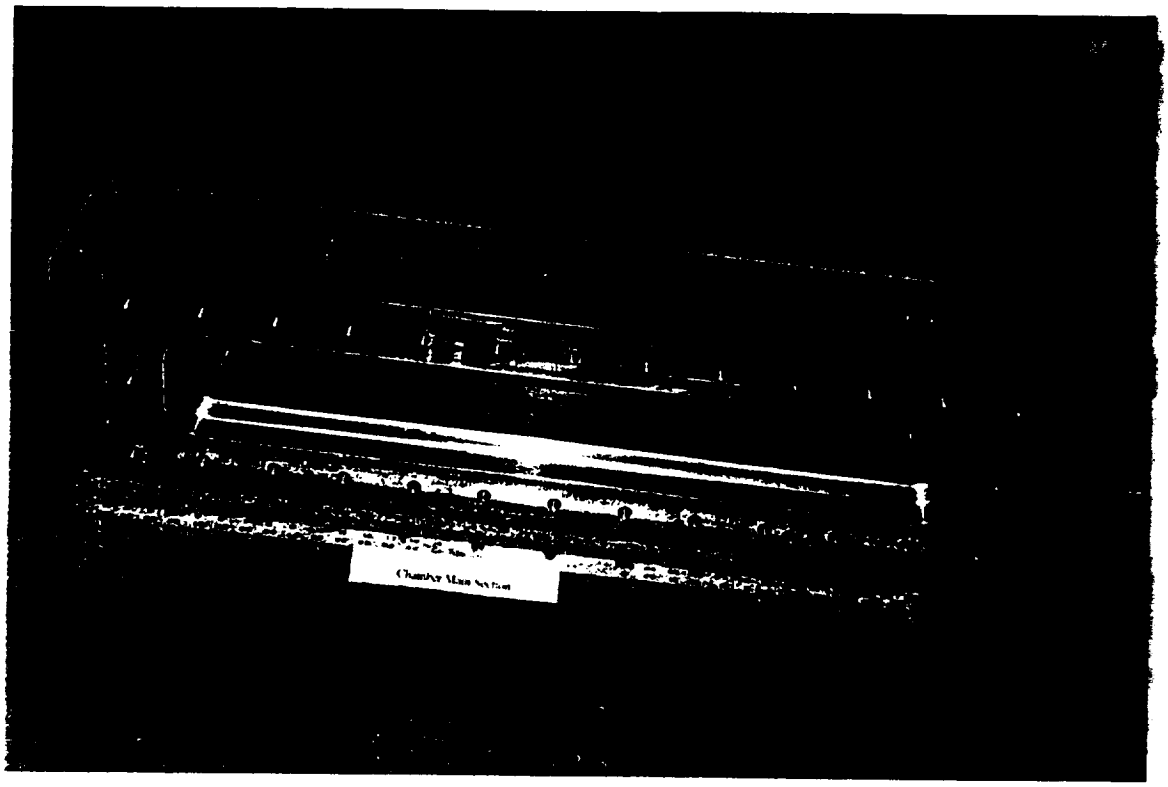

Figure 4. Chamber Main Section

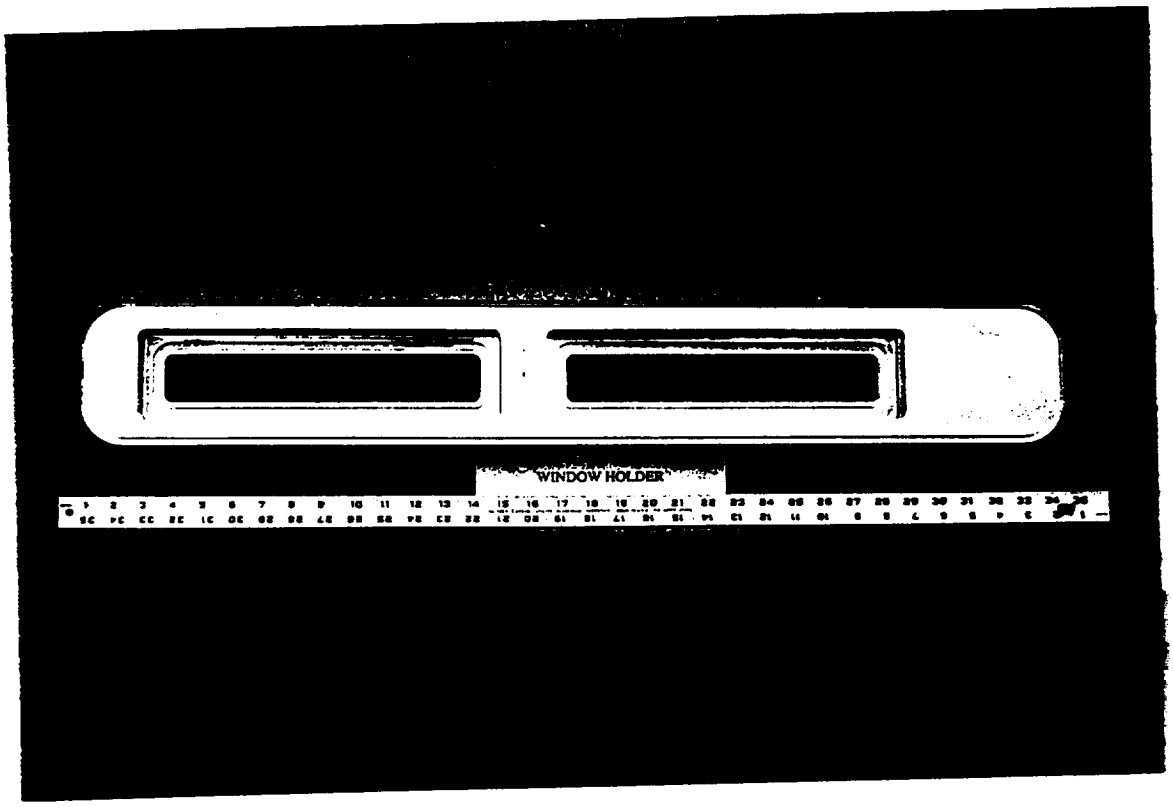

Figure 5. Window Holder

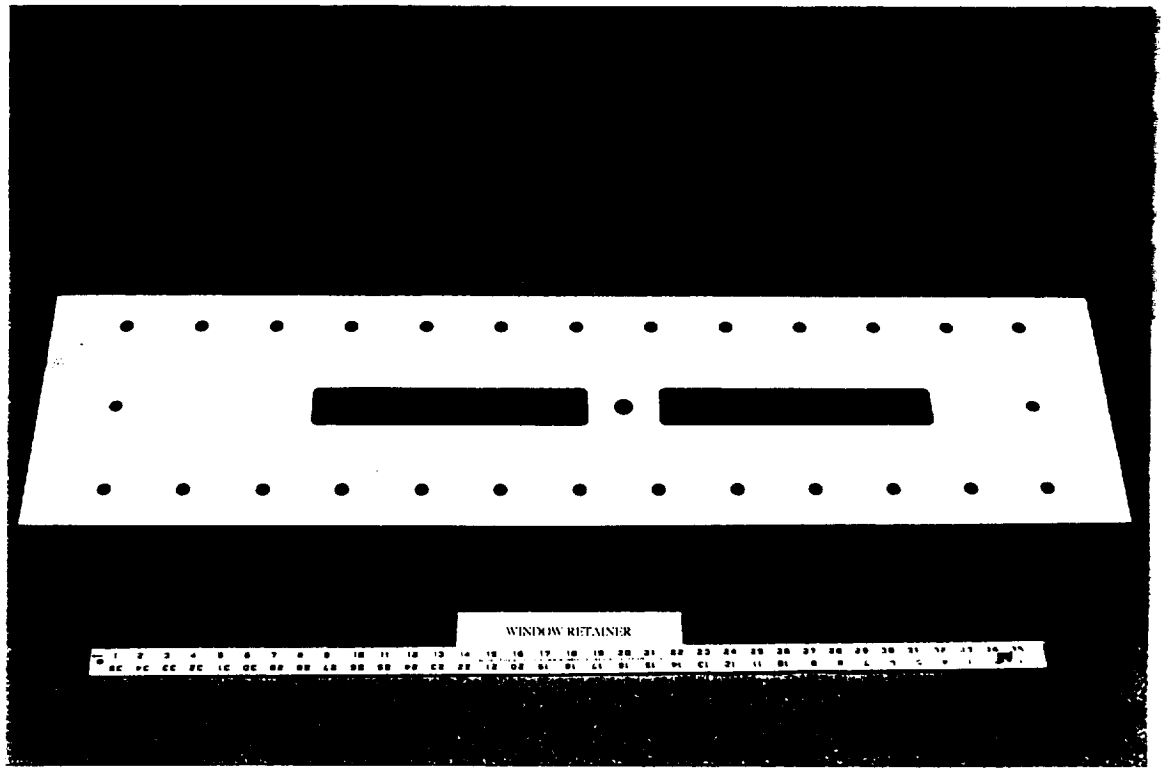

Figure 6. Window Retainer

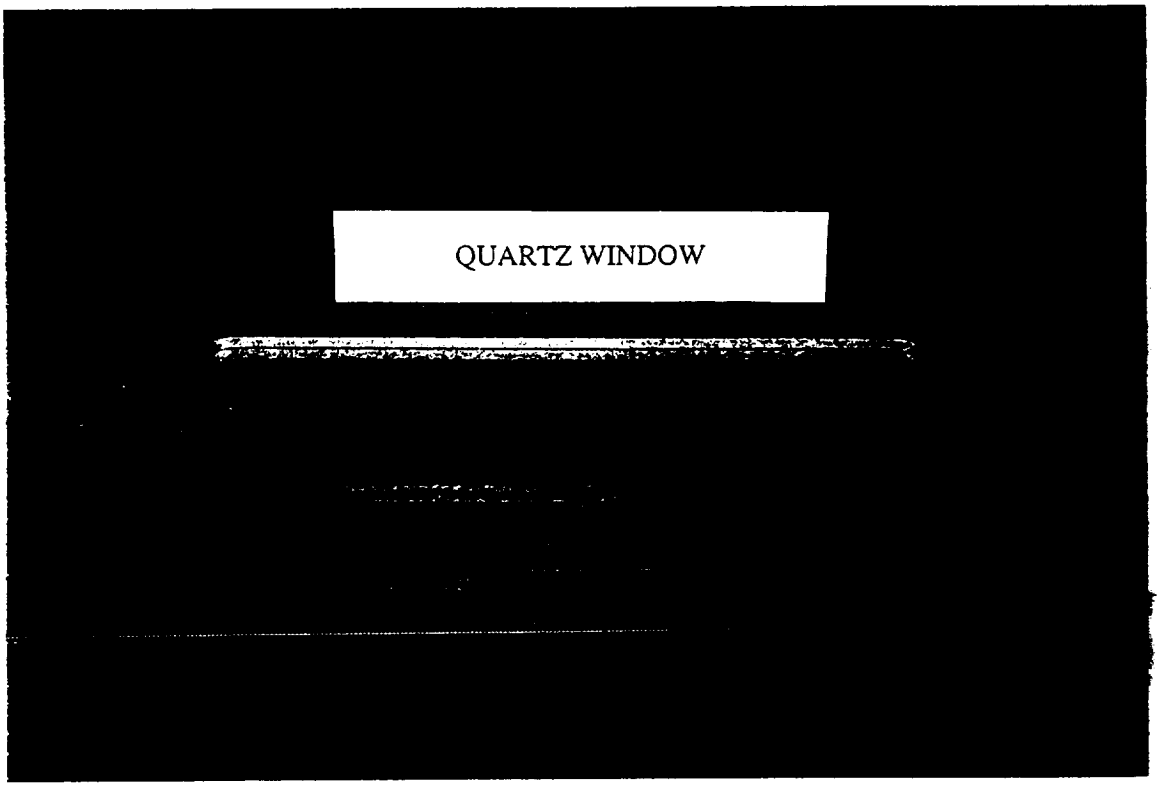

Figure 7. Quartz Window

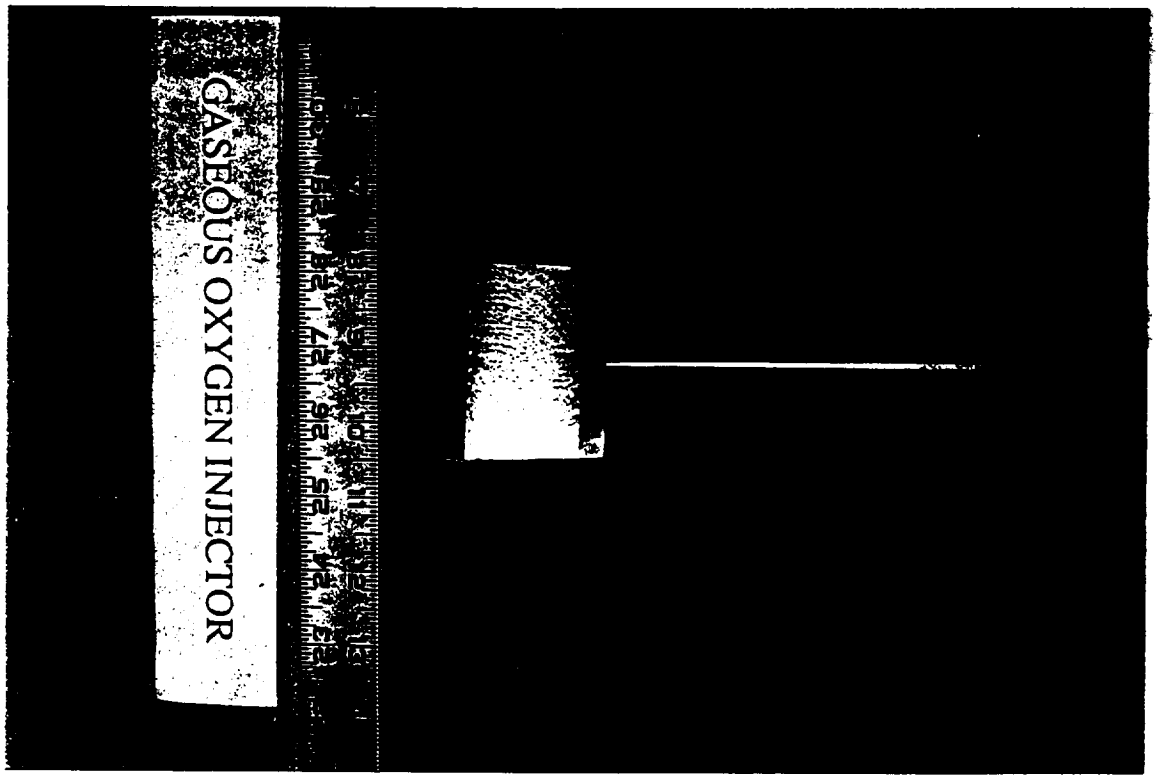

Figure 8. Gaseous Oxygen Injector

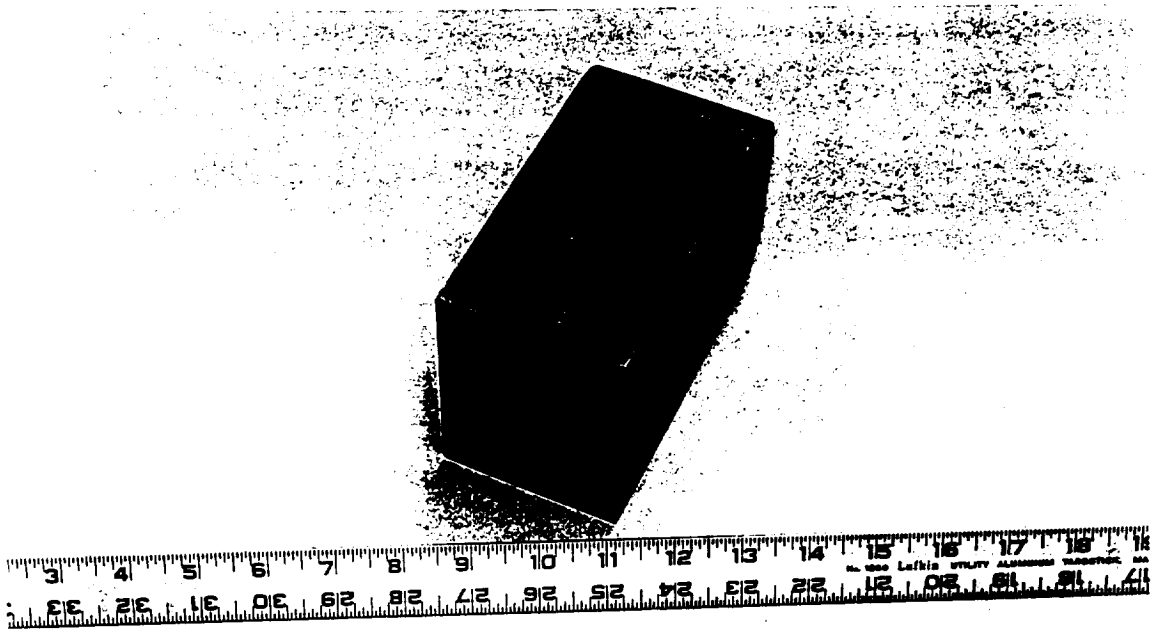

Figure. 9 Graphite Pre–Nozzle Mixing Chamber

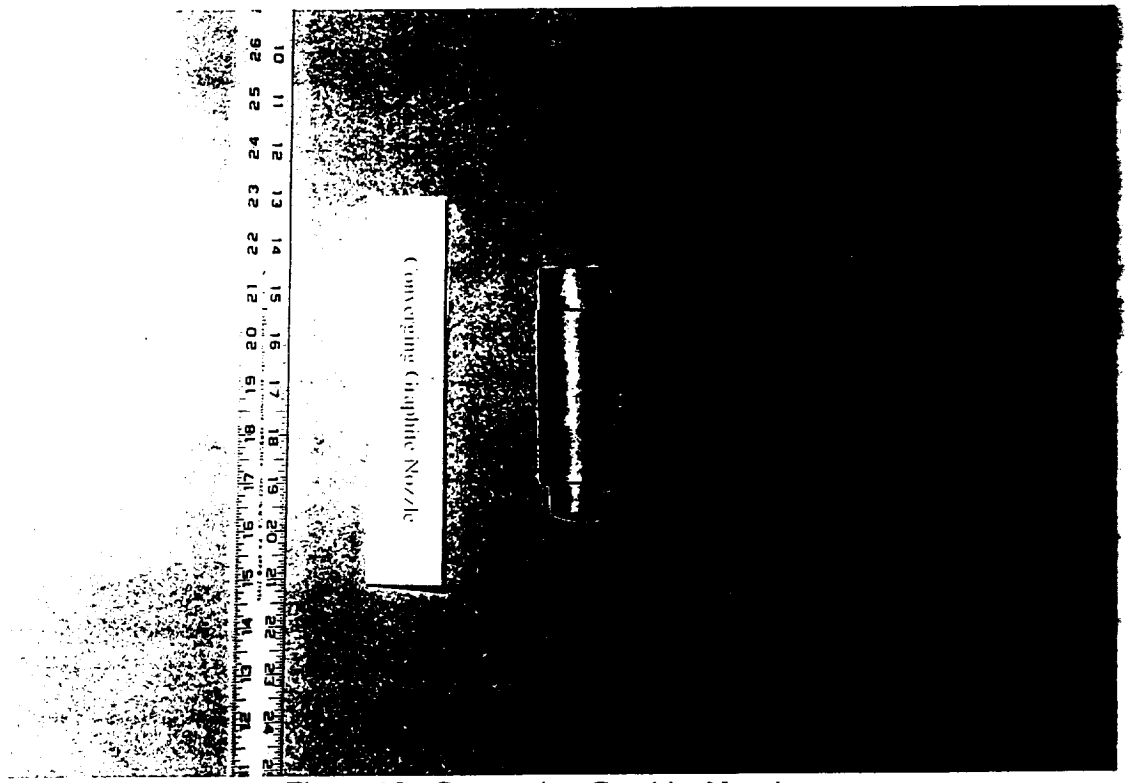

Figure 10. Converging Graphite Nozzle

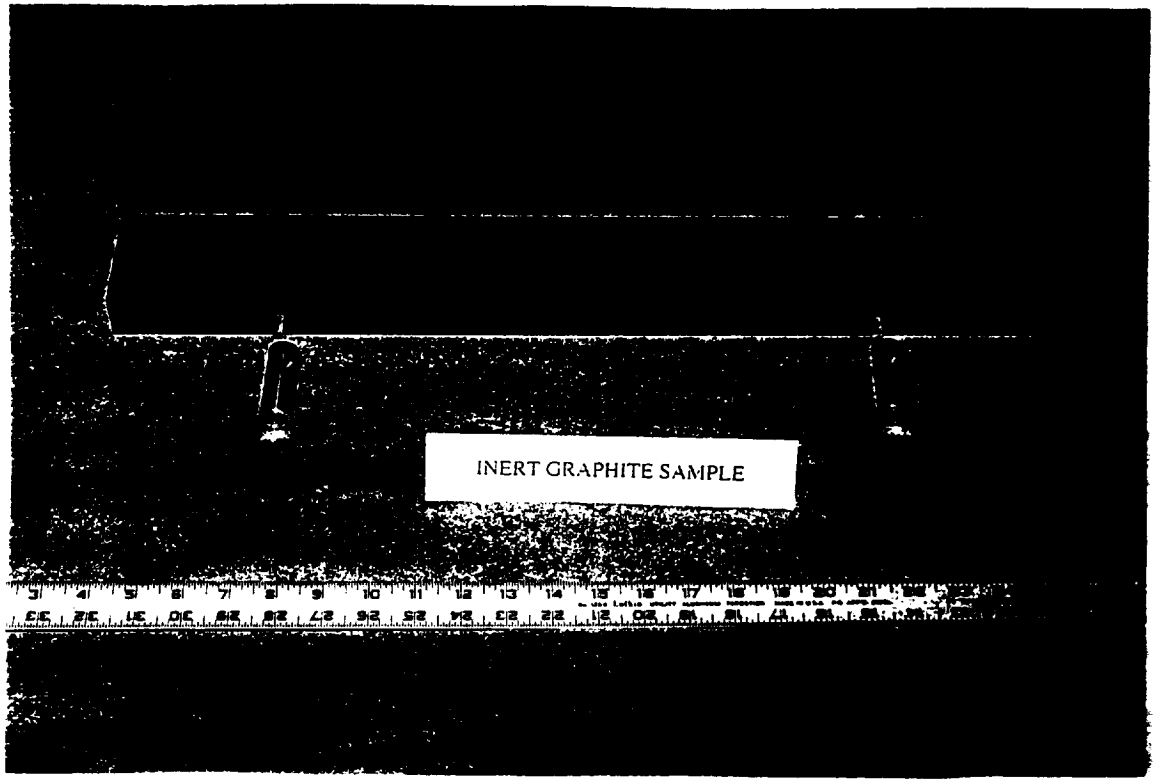

Figure 11. Inert Graphite Sample

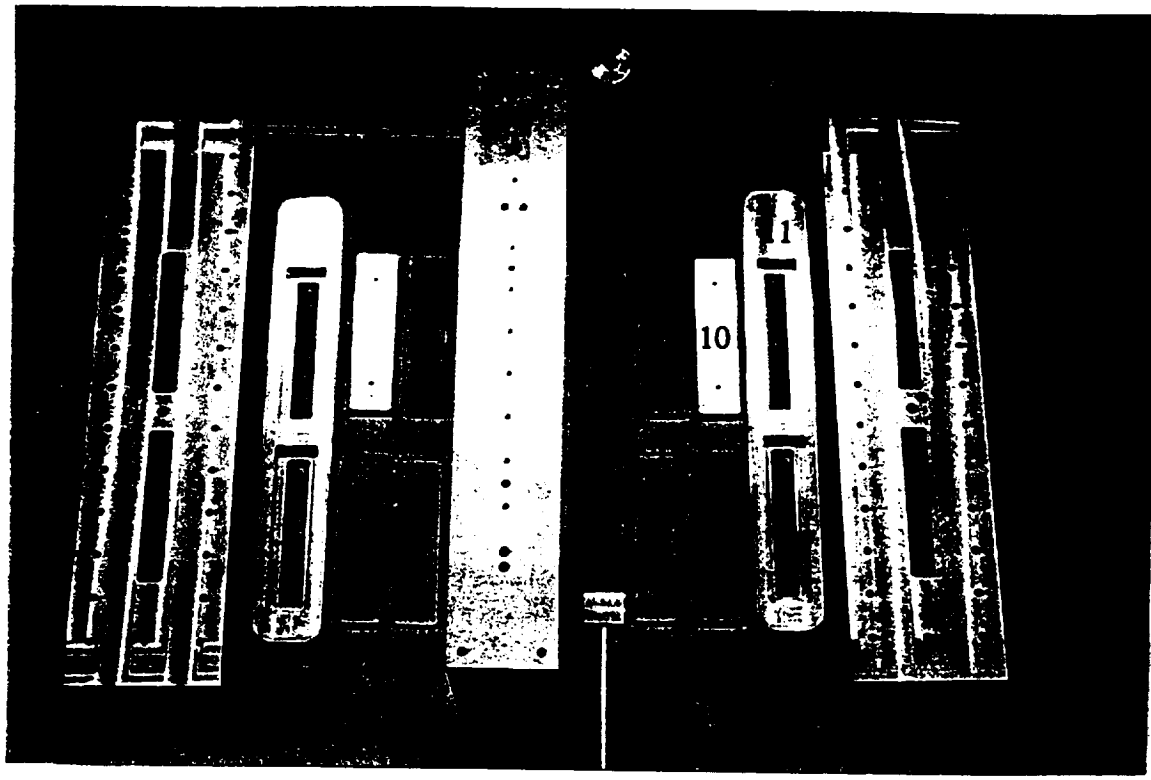

1–Chamber Main Section
2–GOX Injector
3–Inert Graphite Sample
4–Mixing Chamber
5–Converging Exit Nozzle
6–Nozzle Retaining Ring
7–Quartz Window
8–Lexan Window
9–Graphite Window
10–Steel Window
11–Window Holder
12–Window Retaine

Figure 12. Exploded View of Hybrid Motor Analog

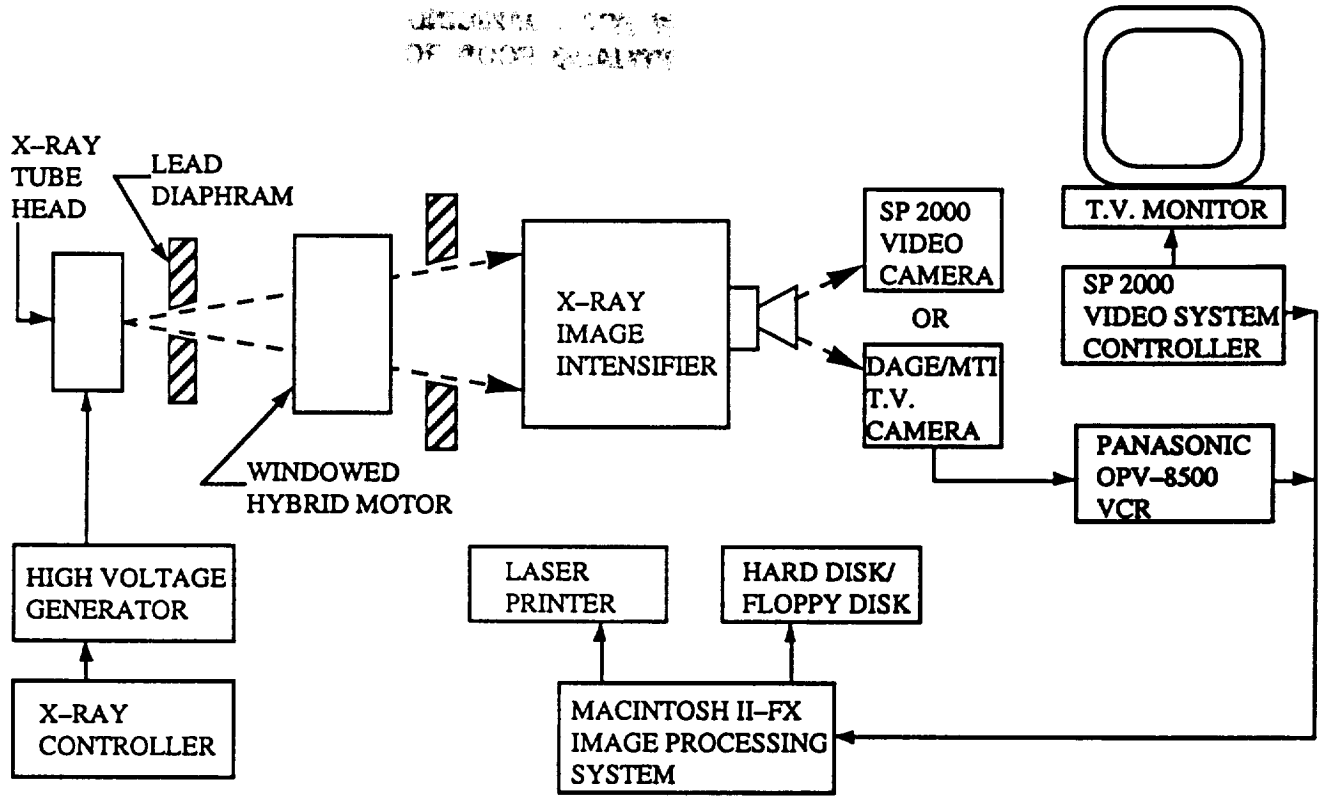

Figure 13. Real-Time X-Ray Radiography System

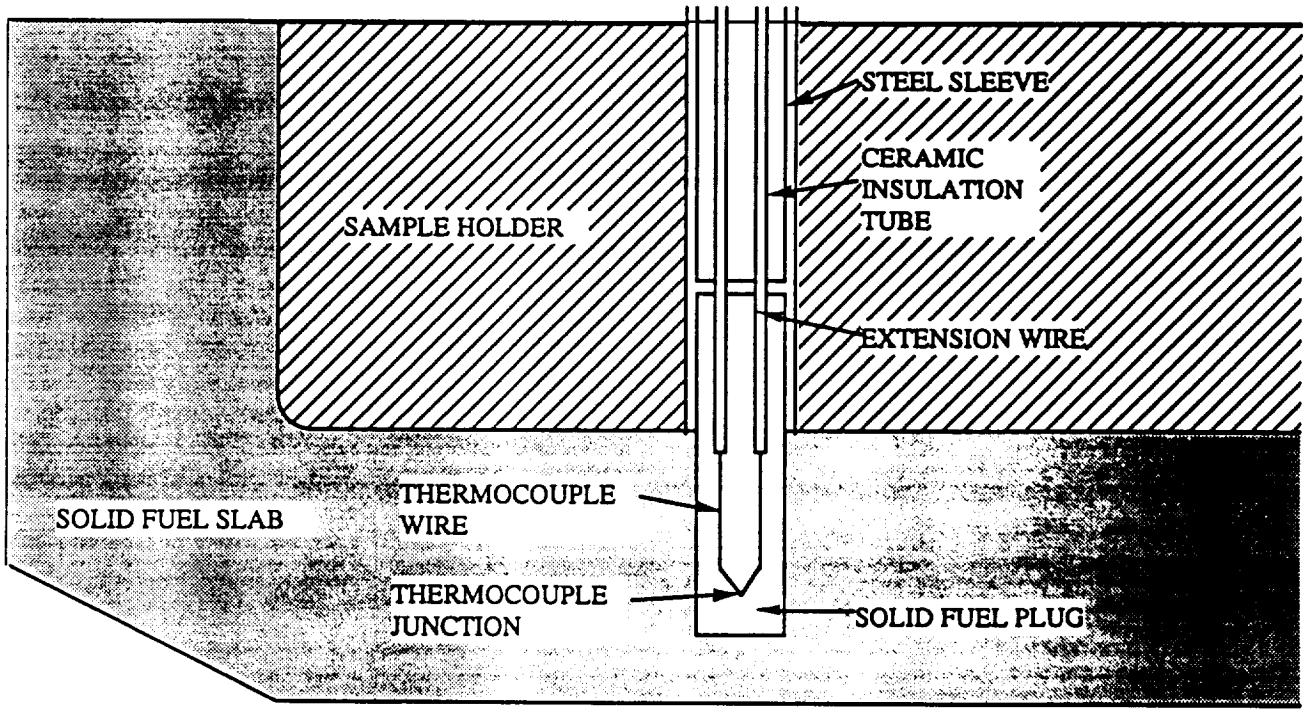

Figure 14. Fine-Wire Thermocouple Embedded in Solid Fuel Slab

Fundamental Phenomena on Fuel Decomposition and Boundary Layer Combustion Processes with Applications to Hybrid Rocket Motors

Semiannual Progress Report

August 2, 1994-November 1, 1994

Task 2: Theoretical Investigation
C. L. Merkle and S. Venkateswaran

1. Introduction

The overall objective is to develop a loosely coupled interface between the reacting gas phase and the solid phase. The work so far has focused on obtaining representative solutions using a simplified coupling model with specified constant fuel surface temperature. Computations have been performed for both axisymmetric and 2D slab geometries. For the gas-phase combustion, HTPB kinetics have been modeled using a global two-step mechanism. Turbulence effects are treated using the standard $k-\epsilon$ model with 'laminar' chemistry. Hitherto, the solid phase is modeled using a simplified burning rate expression or by pre-specifying the burning rate. Parametric studies have been carried out to evaluate qualitative trends as a function of fuel regression rate, fuel surface temperature and chamber pressure. Initial calculations have concentrated on the upstream section of the fuel slab. Presently, these computations have been extended to half-length and full-length of the experimental configuration.

Validation efforts have so far considered turbulent, reacting shear layer computations of a hydrogen-air shear layer experiment from NASA/LeRC and are useful in assessing the capability of the turbulence model in diffusion flames. Initial comparisons with the slab-burner tests are anticipated in the following quarter. A closely-coupled coupled gas-phase/solid phase model using one-dimensional thermal conduction in the solid will also be extensively tested in this period. More detailed modeling of the near-surface decomposition will be included as per experimental evidence.

In the current report, we first present a brief description of the gas-phase combustion model and the fuel surface regression rate model. This is followed by a description of the physical set-up that is used in the modeling of the slab

burner experiments. We then present representative solutions of the 2D slab burner calculations. Finally, we discuss our validation efforts of the modeling of turbulence effects in diffusion flames.

2. Gas-Phase and Solid-Phase Models

Our modeling efforts so far have primarily focused on employing a global two-step combustion model for the reacting gas phase. The first step represents the oxidation of the fuel (the pyrolysis product of HTPB has been taken to be constituted entirely of 1,3 butadiene), while the second step represents the oxidation of wet CO,

$$C_4H_6 + 3.5O_2 \longrightarrow 4CO + 3H_2O$$

$$CO + 0.5O_2 \longleftrightarrow CO_2$$

As noted above the second reaction can proceed in both directions. The reaction rates are obtained using Arrhenius rate expressions. In our computations, in order to obtain realistic flame temperatures, we adjust the backward reaction rate in the second step. This results in increased formation of carbon-monoxide and thereby lower flame temperatures. A more detailed reaction set for H/O/C chemistry involving twelve elemental steps is available and will be tested for comparison.

For the solid phase, the fuel surface temperature is specified to be constant (800 K). In addition, the fuel regression rate (or blowing rate) is calculated using an existing pyrolysis model,

$$r_b = A_s exp(-E_a/R_u T)$$

In addition, in many of the calculations, the fuel regression rate is directly specified in order to study the flame characteristics parametrically.

3. Physical Configuration

A typical grid geometry (size 101 X 61) used in the computations of the experimental slab burner geometry is shown in Fig. 1. The upper section shows

the grid to scale while the lower section is scaled by a factor of ten in the wall-normal direction. The latter view allows the details of the flowfield in the near-wall region to be depicted more clearly and is used in the results section for this reason. The particular configuration shown corresponds to a period that is about halfway through the burn. Further, only one-half length of the full length of the geometry is shown. The overall L/D for the case shown is about 10. The location where the grid is stretched strongly in the axial direction corresponds to the leading edge of the fuel slab. The grid is also strongly stretched in the wall normal direction in order to resolve the turbulent boundary layer as well as the details of the flamefront. It should be pointed out that, in these calculations, the details of the forward-facing step upstream of the fuel slab are not included.

Pure gaseous oxygen is specified at the inlet end of the planar geometry. The GOX flow rate is 3.3kg/s and the chamber pressure is between 20 and 60 atm. The inlet GOX temperature is 300K, while the fuel surface temperature is fixed at 800K. The above conditions are representative of the slab burner tests being carried out at Penn State. For the configuration shown in Fig. 1, the inlet GOX mean velocity is about 20 m/s. The fuel surface regression rate was varied between zero blowing to about 20 cm/s. In the following section, typical computational results are presented.

4. Representative Computational Solutions

The computational results shown here correspond to a period that is halfway through the burn. The grid geometry employed is as shown in Fig. 1. The chamber pressure was maintained at 30 atm and the fuel regression rate was 10 cm/s. Figure 2 shows the convergence of the residuals for a typical computation. It can be noted that a relatively small time-step (smaller than the optimum size deduced from linear considerations) was necessary for initializing the computation in a stable fashion. This small value of the time-step is typically maintained anywhere between 1000 and 2000 iterations. Beyond that point, the time-step size may be increased and the associated convergence rate is seen to be extremely rapid. In this case, machine zero is approached in a total of about 4000 iterations.

The choice of small time step size in the initial stages is necessary for a variety of reasons, primarily associated with non-linear effects. However, in this case, the flame was also observed to be unsteady in the initial part of the calculation. Choosing too large of a time-step appeared to intensify the unsteadiness causing the calculation to

blow up. In most cases, however, such a careful flame flowfield initialization is necessary only when a cold start-up is attempted. For further parametric studies, the flowfield may be initialized with an existing solution and usually the optimum time-step size may be selected right away.

Contours of temperature are shown in Fig. 3 both to scale and with the wall normal direction blown up by a factor of ten. The peak temperature in the flame is observed to be about 3600 K. Figure 4 shows an additional set of temperature contours obtained when the wall blowing rate is set to zero. This case corresponds to the limit of pure diffusion of the fuel from the surface. Comparison of Figs. 3 and 4 shows that the flame extends into the core gas to a significantly greater extent for the case with blowing than without. Further, the peak temperature for the zero blowing case is seen to be somewhat lower at about 3300K. This is because the fuel and oxidizer in the latter case are poorly mixed.

Contours of water mass fraction and carbon dioxide are shown in Figs. 5 and 6 corresponding to the case with blowing. The peak CO_2 mass fraction is about 0.6 while that of H_2O is about 0.25. The contours of CO mass fraction (not shown) reveal a peak value of about 0.015. In contrast, the CO mass fractions for the zero blowing case are much higher, again an indication of the poor mixing of the fuel and oxidizer.

5. Validation of Turbulent Reacting Shear Layers

As noted earlier, the flame characteristics are strongly dependent on the degree of mixing between the fuel and oxidizer. In the hybrid rocket motor, the turbulence levels in the boundary layer as well as in the free-stream will strongly influence the degree of mixing and thereby the flame characteristics. Therefore, it is important to carefully assess the performance of the present turbulence model (standard $k - \epsilon$) turbulent diffusion flame computations. This validation study is part of a more general effort within our group to improve our capability of modeling turbulent combustion and is being done in conjunction with other on-going projects.

As an initial step in the validation of turbulent reacting flow simulations, we have considered the hydrogen-air reacting subsonic shear layer experiments conducted at NASA/LeRC. Fig. 7 shows comparison of the computed mean velocity and turbulent kinetic energy profiles compared against experimental data for a non-reacting shear layer. The mean velocity profiles are predicted fairly well, while the turbulent kinetic energy matches the experiments reasonably well in the first few axial stations. Further

downstream, the computed spreading in turbulent kinetic energy is somewhat less than the measurements. This discrepancy is typical of turbulent shear layer computations and may be attributed to flow intermittency arising from large scale vortex structures at the edges of the shear layer.

Computed and experimental results for a reacting shear layer case are shown in Fig. 8. The mean velocity profiles are again reasonably well-predicted, while the turbulent kinetic energy profiles agree quite poorly. It should be noted that the turbulent kinetic energy is significantly in error even at the first axial location which is close to the inlet of the experimental chamber. This discrepancy, associated with poor characterization of the inlet turbulence levels, is probably responsible for the poor agreement at the downstream stations as well. Parametric study of the effects of varying inlet turbulence levels are planned and will be useful in establishing the need for more improved turbulence models.

6. Plans for the Next Quarter

Validation efforts of turbulent reacting flow computations will continue. In particular, parametric effects of free-stream turbulence levels on shear-layer and flame characteristics will be studied both for the LeRC shear layer experiments as well as for the HTPB slab burner tests being carried out at Penn State. In the following quarter, we anticipate making preliminary comparisons with experimental measurements from the slab burner tests. The computational model will be enhanced by a more detailed modeling of the solid phase. Furthermore, enhancements to the surface decomposition model will be addressed.

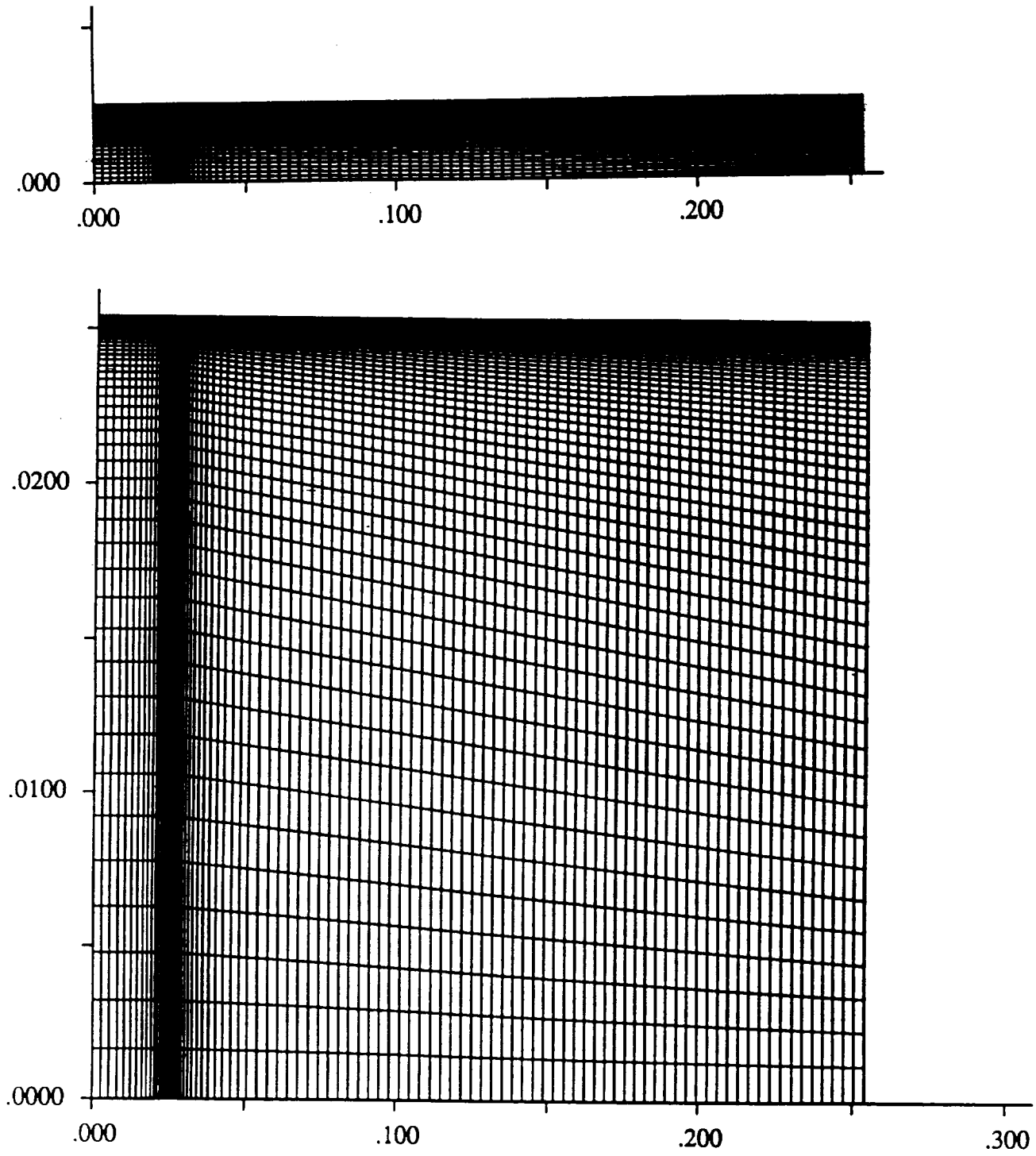

Figure 1 Typical grid geometry used for 2D planar slab burner configuration. Grid size is 101 X 61. Upper figure shows grid to scale. Lower figure shows y-coordinate scaled by a factor of ten.

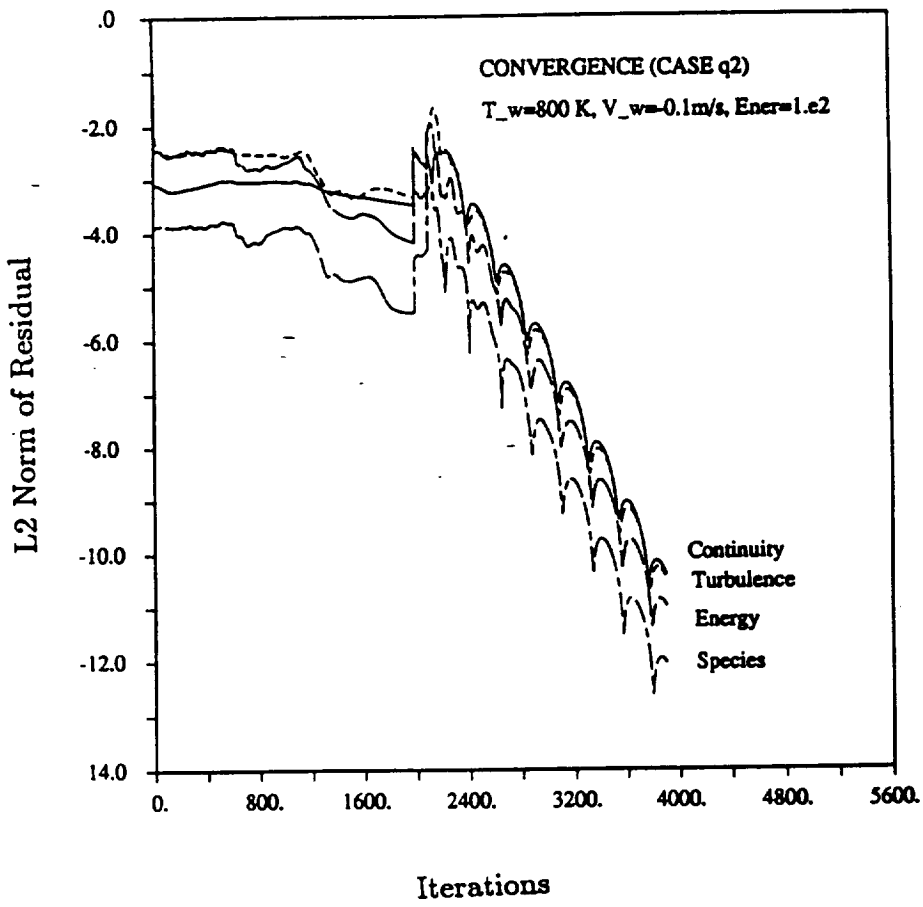

Figure 2 Convergence of representative computation. Chamber pressure is 30 atm. Wall temperature is 800 K. Wall blowing rate is 10 cm/s.

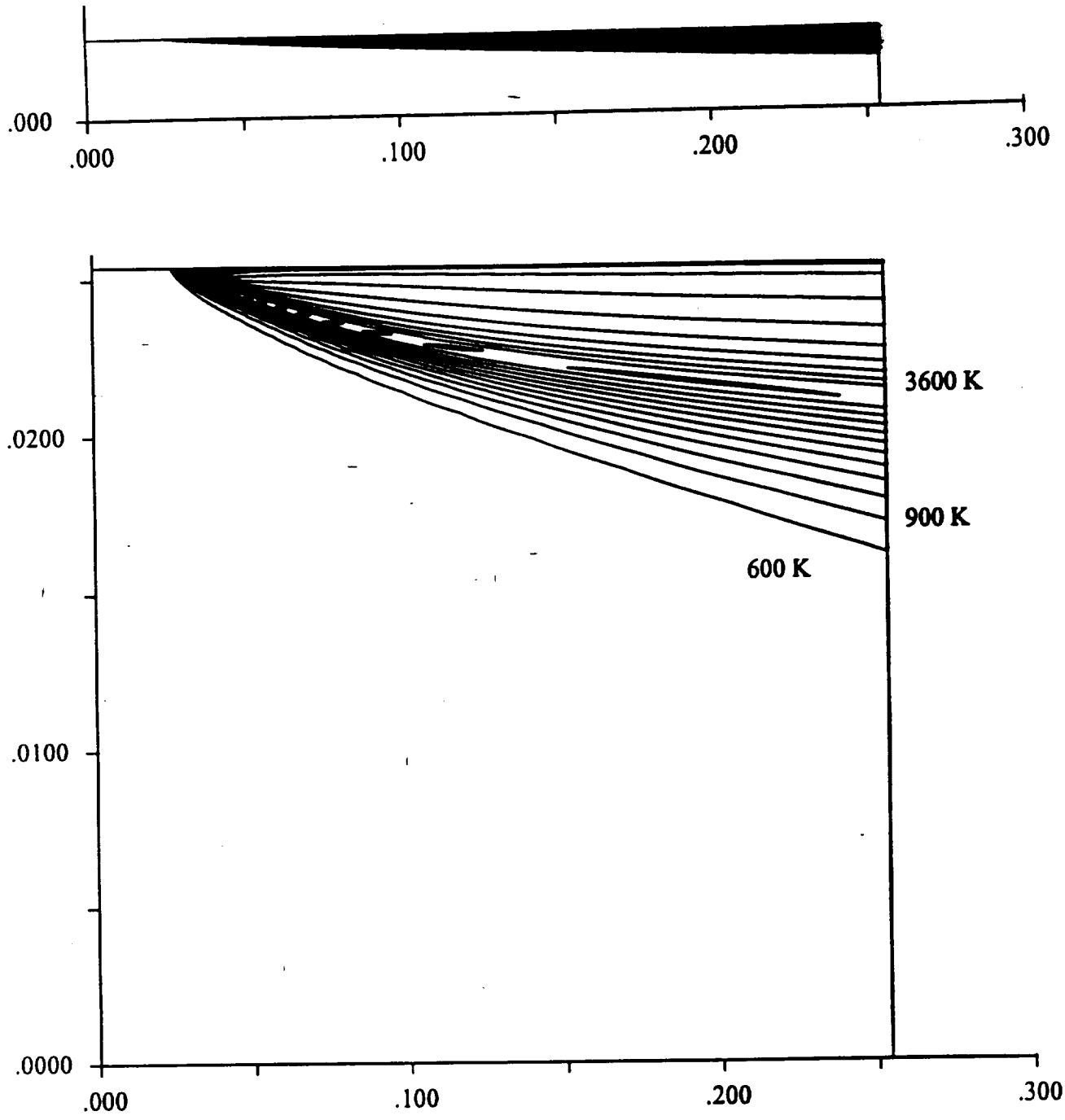

Figure 3 Temperature contours in slab burner geometry. Chamber pressure is 30 atm. Wall temperature is 800 K. Wall blowing rate is 10 cm/s.

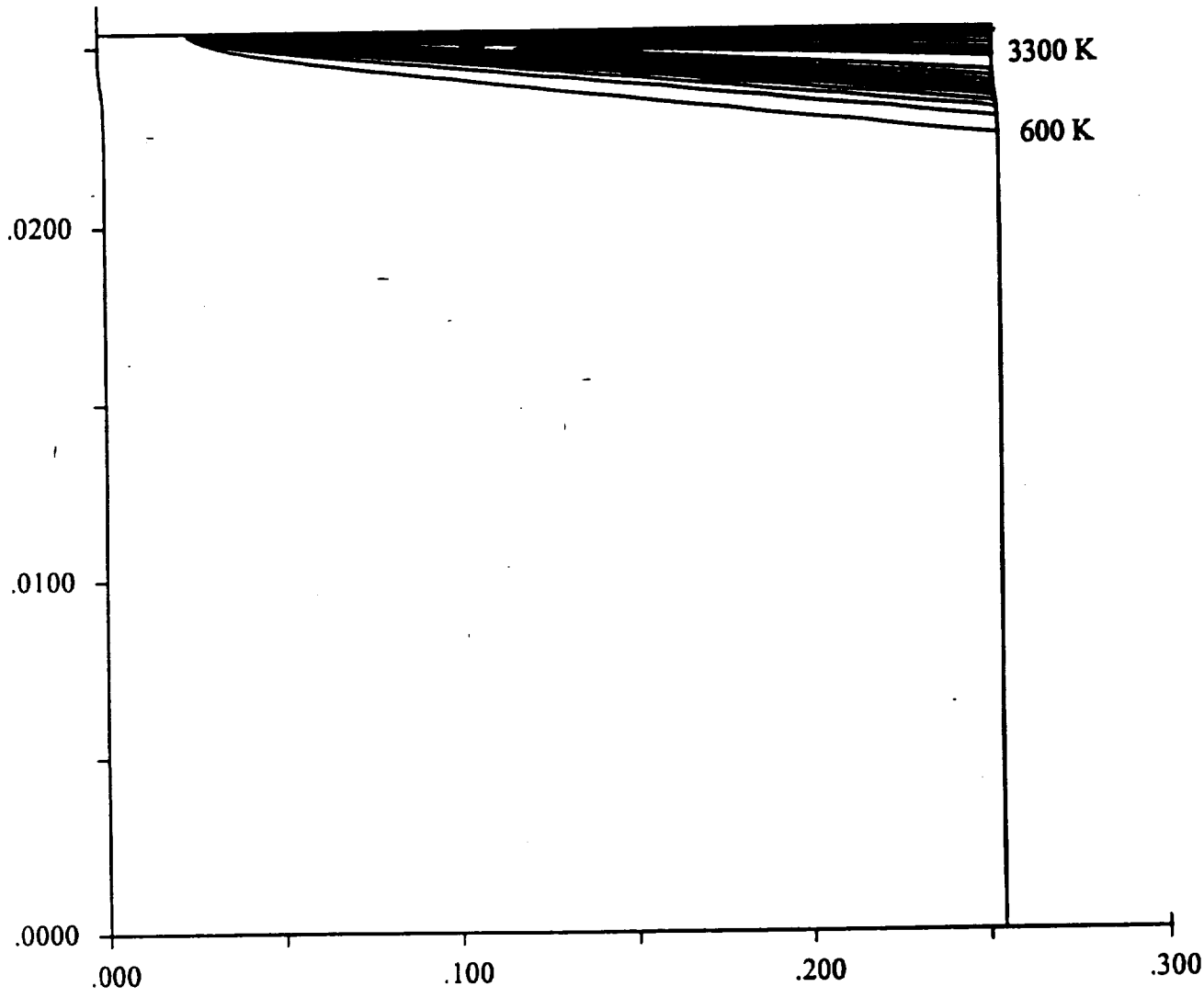

Figure 4 Temperature contours in slab burner geometry. Chamber pressure is 30 atm. Wall temperature is 800 K. Zero wall blowing rate.

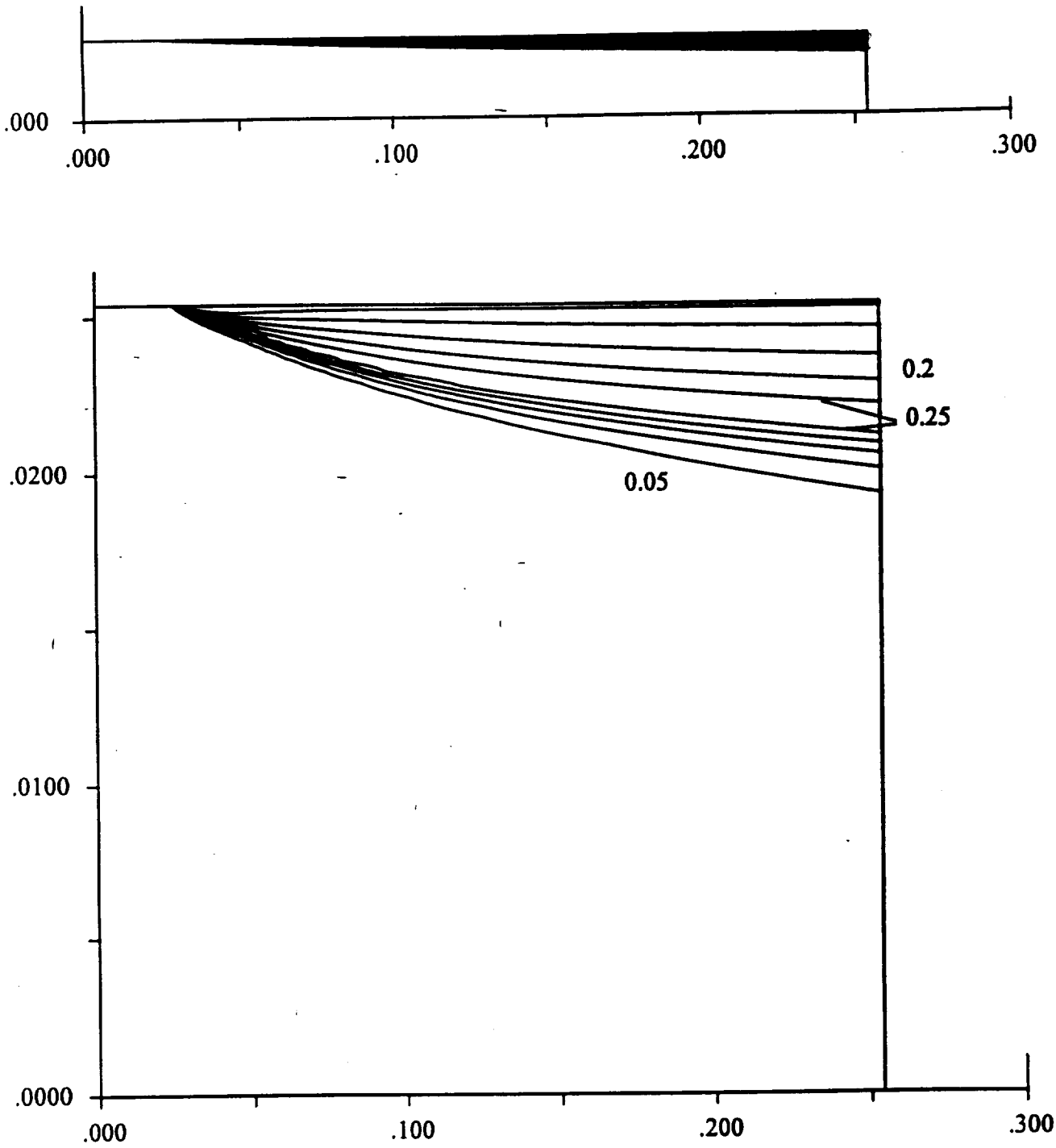

Figure 5 Water mass fraction contours in slab burner configuration. Chamber pressure is 30 atm. Wall temperature is 800 K. Wall blowing rate is 10 cm/s.

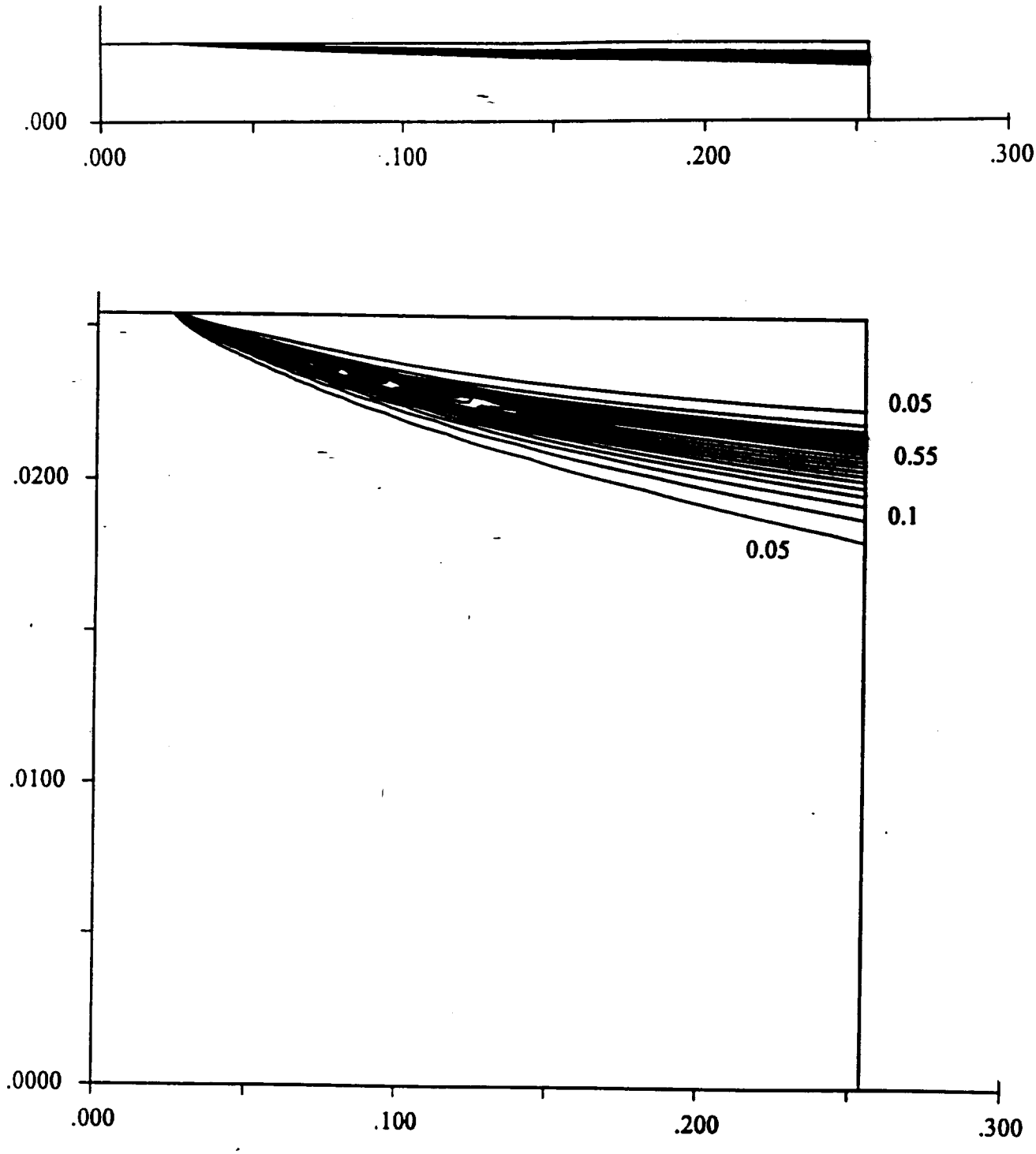

Figure 6 Carbon dioxide contours in slab burner configuration. Chamber pressure is 30 atm. Wall temperature is 800 K. Wall blowing rate is 10 cm/s.

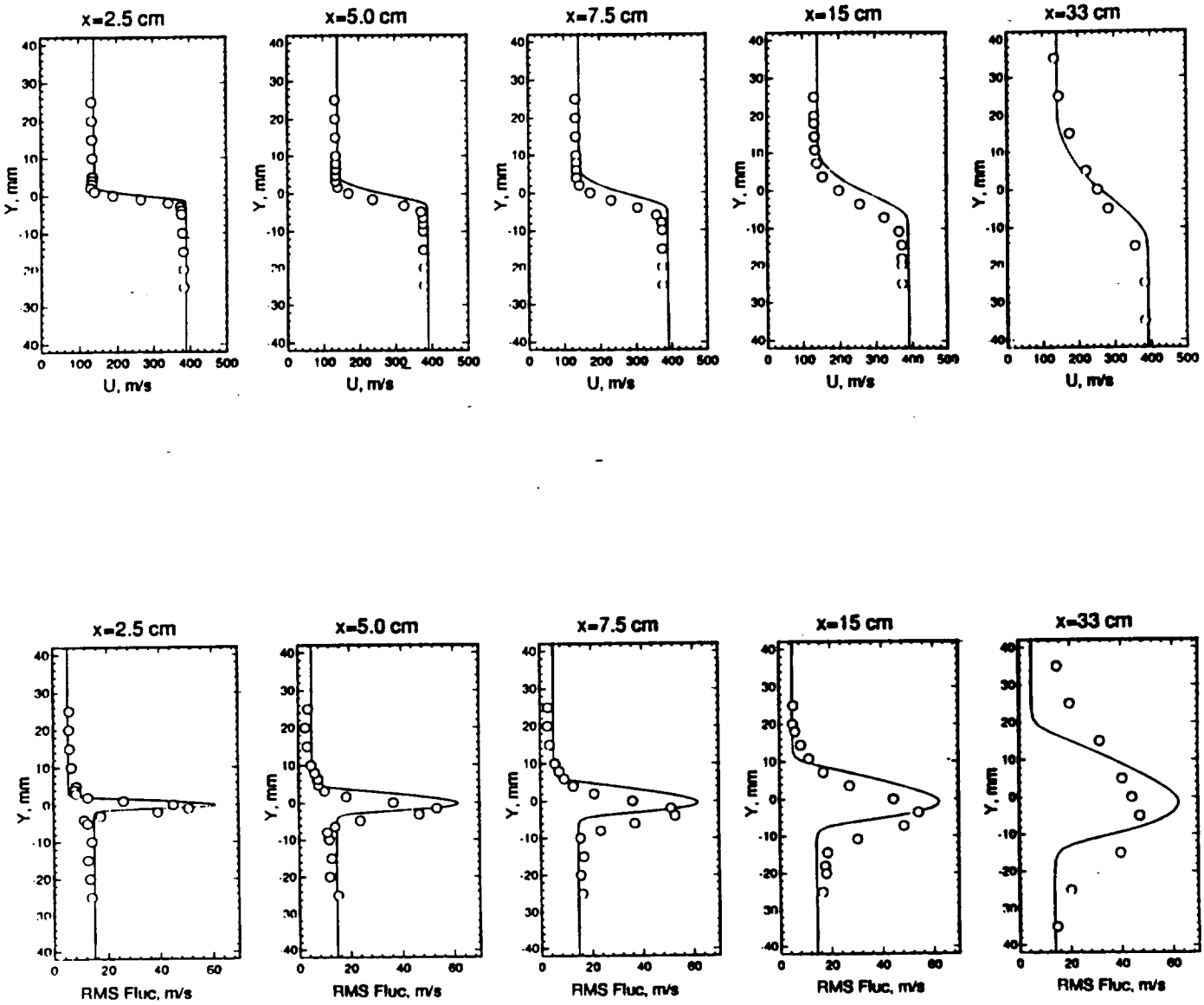

Figure 7 Non-reacting shear layer results. Top figure shows computed and measured mean velocity profiles. Bottom figure shows computed and measured turbulence kinetic energy.

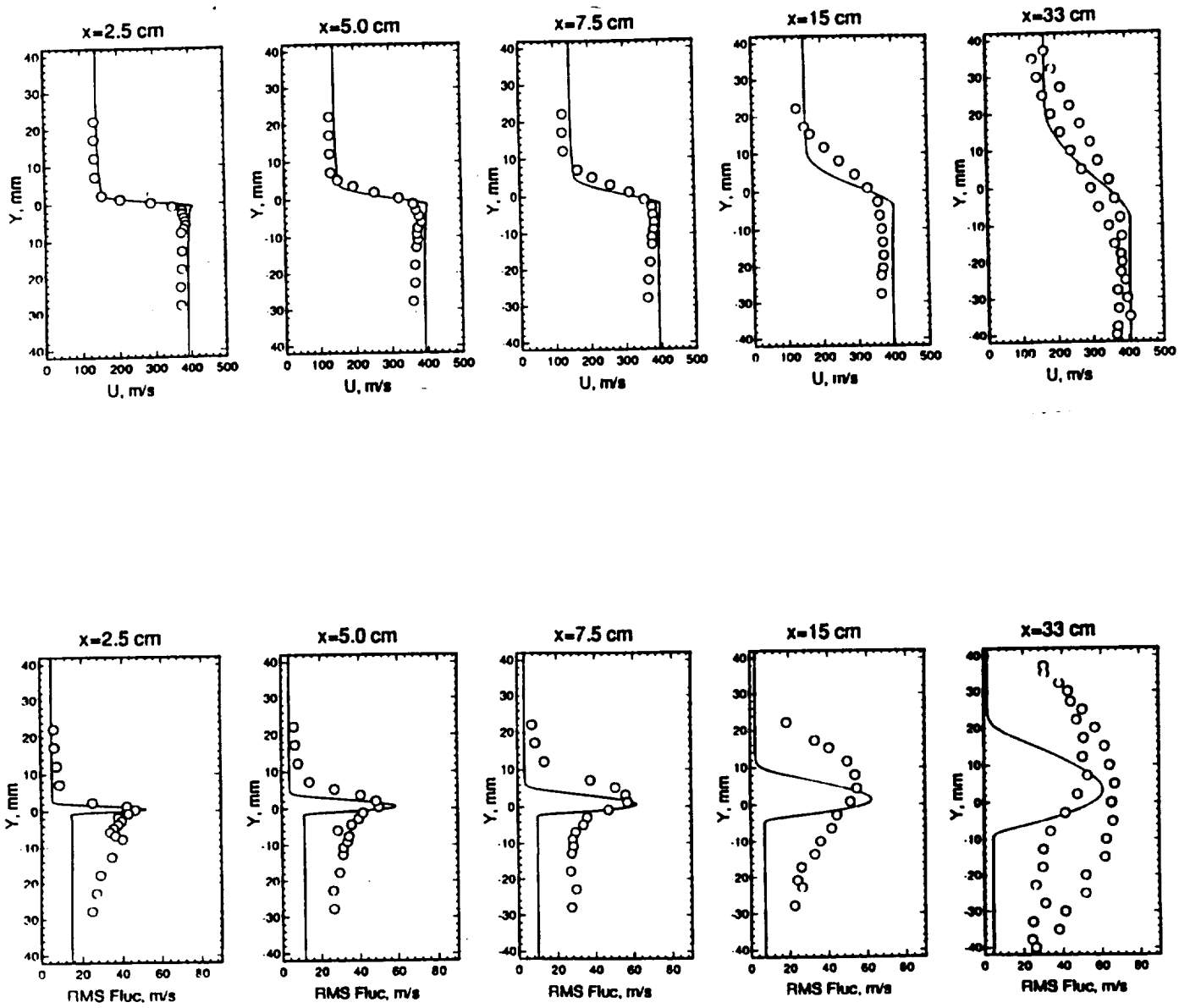

Figure 8 Reacting (hydrogen-air) shear layer results. Top figure shows computed and measured mean velocity profiles. Bottom figure shows computed and measured turbulence kinetic energy.